ADVANCED FUNCTIONAL MATERIALS
www.afm-journal.de

17.2% Efficiency for Completely Non-Fused Acceptor Organic Solar Cells Via Re-Intermixing Strategy in D/A Stratified Active Layer

Xiyun Xie, Ruijie Ma, Sen Zhang, Top Archie Dela Peña, Yongmin Luo, Zixuan Huang, Tao Jia, Jiaying Wu, Qunping Fan, Wei Ma, Aung Ko Ko Kyaw,* and Gang Li**

Pursuing power conversion efficiency (PCE) is the priority of developing organic solar cells (OSCs) based on low-cost completely non-fused ring acceptors. Herein, a donor/acceptor re-intermixing strategy to enhance the photon capturing process, based on a previously established well-stratified active layer morphology is reported. By adding 20 wt% PTQ10 (polymer donor) into the acceptor's precursor, the device PCE is increased to 16.03% from 15.11% of the D18/A4T-16 control system, which is attributed to the additional charge generation interface and suppressed bimolecular recombination. On the contrary, using the equal ratio of PM6 leads to significant efficiency loss, indicating the importance of considering vertical distribution from the perspective of thermodynamics. Moreover, a cutting-edge level of 17.21% efficiency for completely non-fused ring acceptor systems is realized by altering the active layer to PBQx-TF/TBT-26 and PTQ11, via the identical processing strategy. This work thus presents attractive device engineering and solar cell performance, as well as in-depth vertical morphology understanding.

1. Introduction

The power conversion efficiency (PCE) of organic solar cells (OSCs) has surpassed 20% in both single-junction and tandem structured devices, thanks to the synergistic advance in material design and fabrication optimization.[1–13] Simultaneously, the operational stability of OSCs has been reported with year-scale T_{80} lifetime,[14–20] indicating that this clean energy harvesting technology is nearing commercialization. However, these advances rely on fused ring acceptor materials with complicated chemical structures, which are synthesized from expensive ingredients and have low yields.[21–24] Therefore, developing OSCs based on non-fused ring acceptors is a more promising path toward commercialization despite the significantly lower device efficiency.[25–33]

Aside from designing new high-performance materials, optimizing the active layer morphology by adjusting solution deposition details is crucial for promoting the PCE. Techniques such as additive engineering, sequential deposition, and ternary blend construction have proven effective.[34–42] In our previous work, we utilized the poor solubility of D18 (Poly[(2,6-(4,8-bis(5-(2-ethylhexyl-3-fluoro)thiophen-2-yl)-benzo[1,2-b:4,5-b′]dithiophene))-alt-5,5′-(5,8-bis(4-(2-butyloctyl)thiophen-2-yl)dithieno[3′,2′:3,4;2″,3″:5,6]benzo[1,2-c][1,2,5]-

X. Xie, R. Ma, G. Li
Department of Electrical and Electronic Engineering
Research Institute for Smart Energy (RISE)
Photonic Research Institute (PRI)
The Hong Kong Polytechnic University
Hong Kong 999077, China
E-mail: ruijie.ma@polyu.edu.hk; gang.w.li@polyu.edu.hk

X. Xie, A. K. K. Kyaw
Guangdong University Key Laboratory for Advanced Quantum Dot Displays and Lighting Department of Electrical & Electronic Engineering
Southern University of Science and Technology
Shenzhen 518055, China
E-mail: aung@sustech.edu.cn

The ORCID identification number(s) for the author(s) of this article can be found under https://doi.org/10.1002/adfm.202411286

S. Zhang, Q. Fan, W. Ma
State Key Laboratory for Mechanical Behavior of Materials
Xi'an Jiaotong University
Xi'an 710049, China

T. A. Dela Peña, Y. Luo, J. Wu
The Hong Kong University of Science and Technology
Function Hub
Advanced Materials Thrust
Nansha, Guangzhou 511400, China

Z. Huang
School of Life Science
South China Normal University
Guangzhou 510631, China

T. Jia
School of Optoelectronic Engineering
Guangdong Polytechnic Normal University
Guangzhou 510665, China

DOI: 10.1002/adfm.202411286

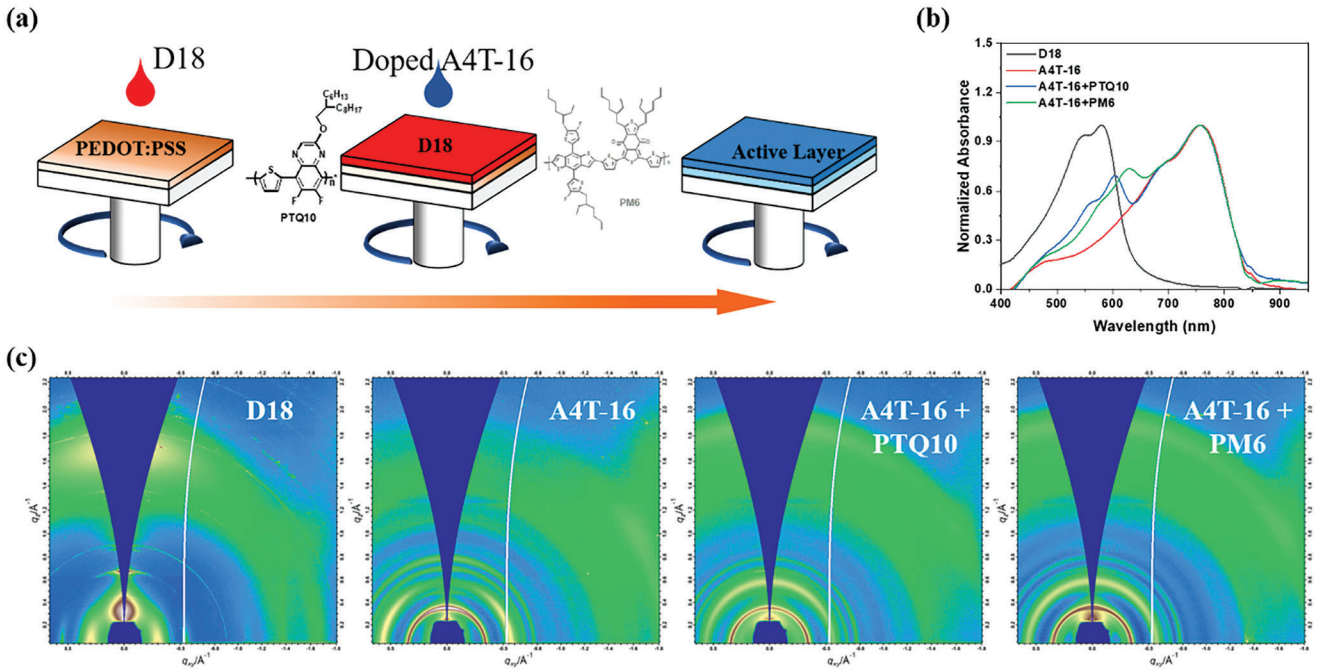

Figure 1. a) Illustration of LBL fabrication process. b) UV–vis absorption spectra of D18 and A4T-16 neat films, as well as PTQ10 and PM6 incorporated A4T-16 films. c) Corresponding 2D-GIWAXS patterns.

thiadiazole)]) in ortho-xylene (o-XY) to achieve a partially intermixed and well-stratified donor–acceptor vertical distribution via layer-by-layer (LBL) processing. This morphology yielded a decent PCE of 15% for an optimal thin-film (100 nm) device, the corresponding devices exhibited a thickness-insensitive characteristic.[43] However, this kind of method may result in insufficient charge generation since the donor–acceptor blending region is not as abundant as in the films produced by the one-step casting method, leading to lower photon capture.

Inspiringly, a recent report proposed a dilution strategy for both donor and acceptor deposition on LBL fabricated active layer, which significantly boosts both short-circuit current density (J_{SC}) and fill factor (*FF*), without sacrificing open-circuit voltage (V_{OC}).[44] Accordingly, for our cases, properly introducing polymer donor materials (soluble in o-XY) should facilitate forming an additional donor–acceptor intermixing phase in an acceptor-rich region, thereby improving device performance. Therefore, in this study, we utilized two representative commercially available polymer donors, PTQ10 (Poly[[6,7-difluoro[(2-hexyldecyl)oxy]−5,8-quinoxalinediyl]−2,5-thiophenediyl]]) and PM6 (Poly[(2,6-(4,8-bis(5-(2-ethylhexyl-3-fluoro)thiophen-2-yl)-benzo[1,2-b:4,5-b']dithiophene))-alt-(5,5-(1′,3′-di-2-thienyl-5′,7′-bis(2-ethylhexyl)benzo[1′,2′-c:4′,5′-c']dithiophene-4,8-dione)]), proven efficient in previous study,[45] to optimize the device performance of host system D18/A4T-16. As a result, 20 wt% PTQ10 (optimized) doping in A4T-16-layer leads to a PCE increase from 15.11% (control device) to 16.03%, while 20 wt% PM6 results in a much lower efficiency of 12.78%. A series of morphological characterizations reveal that the crystallization tuning effects of PTQ10 and PM6 on A4T-16 are very similar, but excessively high surface tension of PM6 results in unfavorable vertical phase segregation, inhibiting initial charge generation and transport. In contrast, PTQ10 enriches the top part of the film, providing an additional charge-generating region. Photophysical experiments point out that PTQ10incorporation can enhance the polaron generation and hole transfer process while suppressing the free charge carrier recombination. Furthermore, by replacing A4T-16 with another high-performing completely non-fused ring acceptor, TBT-26,[46] we achieved a state-of-the-art PCE of 17.21% using the PBQx-TF (Poly[(2,6-(4,8-bis(5-(2-ethylhexyl-3-fluoro)thiophen-2-yl)-benzo[1,2-b:4,5-b']dithiophene))-alt-5,5′-(6,9-bis(4-(2-butyloctyl)thiophen-2-yl) dithieno[3,2-f:2′,3′-h]quinoxaline)])/TBT-26 system with 20 wt% PTQ11 (Poly[(thiophene)-alt-(6,7-difluoro-2-(2-hexyldecyloxy)−3-methylquinoxaline]).

2. Results and Discussion

The bottom D18 layer and upper A4T-16 or PTQ10-doped A4T-16 or PM6-doped A4T-16 layer were fabricated by the LBL process according to previous reports.[47–50] The fabrication process and the chemical structures of utilized materials are illustrated in **Figure** 1a. First, we investigated the aggregation characteristics of the various LBL-processed films from their UV–vis absorption spectra (Figure 1b; Figure S1, Supporting Information).[51–53] In film-state, even the highly crystalline D18 demonstrates a considerable amorphous signal, while its 0-0 and 0–1 vibrational peaks are also significant. Compared with neat acceptor film, PTQ10 and PM6 (20 wt%) incorporated films demonstrate improved ordered aggregation ratios as 0-0 vibrational peak becomes dominant. Furthermore, the PM6 introduction leads to a more suppressed 0–1 vibrational peak than PTQ10 does, indicative of its better interaction with A4T-16.

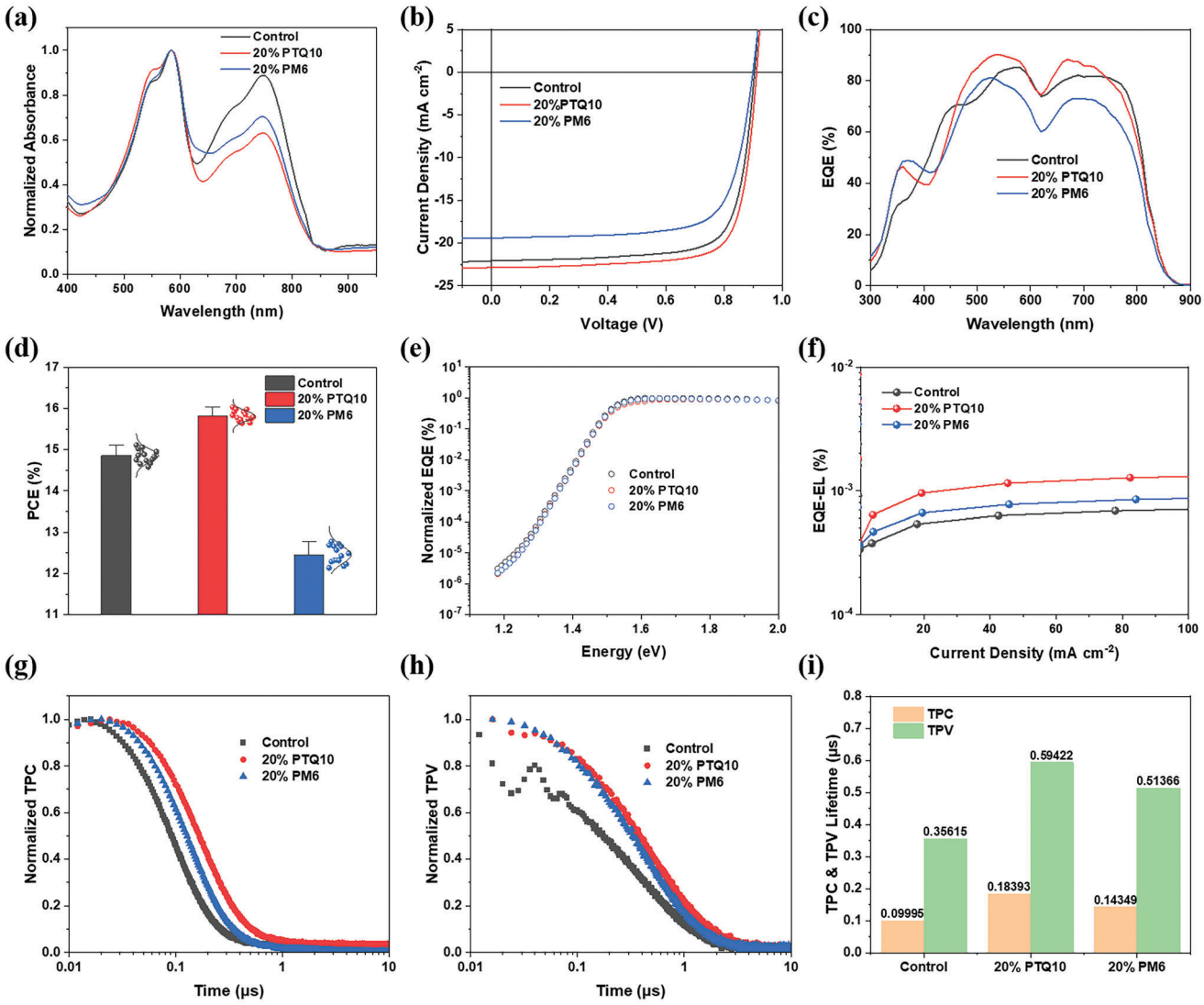

Figure 2. a) UV–vis absorption profiles of D18/A4T-16 control film, 20% PTQ10, and 20% PM6 incorporated films. b) *J–V* characteristics, c) EQE spectra, and d) normal distribution of PCEs for the three systems. e) FTPS-EQE and f) EQE-EL data for the energy loss analysis. g) TPC and h) TPV curves, and i) derived lifetime values.

Next, the molecular packing and crystallization of the bottom and top layers in device fabrication are investigated by grazing-incidence wide-angle X-ray (GIWAXS) test.[54–56] The corresponding 2D patterns and extracted line-cuts alongside in-plane (IP) and out-of-plane (OOP) directions are displayed in Figure S2 (Supporting Information). The fitting parameters, including d-spacing and coherence length (CL) values, are summarized in Tables S1 and S2 (Supporting Information). Consistent with previous findings, D18 exhibits a strong crystallinity, evidenced by distinct diffraction peaks and its well-known face-on orientation.,[57] In contrast, A4T-16 exhibits an edge-on orientation and other isotropic diffraction peaks. When PTQ10 and PM6 are added, the edge-on feature of the A4T-16 host film is reduced, indicating suppression of characteristic small molecule crystallization. Interestingly, the addition of 20% PTQ10 leads to the disappearance of π–π stacking signals in the IP direction, while its OOP (010) peak becomes recognizable. The 20% PM6-doped A4T-16 film also shows a π–π stacking peak in the OOP direction, suggesting that both polymer donors modulate the crystallization and aggregation of the A4T-16 host film similarly. Furthermore, the experimental results confirm that π–π stacking peak of A4T-16 is located at ≈1.85 $Å^{-1}$, different from D18's peak at 1.67 $Å^{-1}$, providing useful information for analyzing blend film morphology.

After clarifying the morphologic and optoelectronic properties of the bottom and top layers, we examined the combined active layer and related device performance. First, the UV–vis absorption profiles of blend films based on D18/A4T-16 (denoted as the control for D18/A4T-16, 20% PTQ10 for D18/20 wt% PTQ10-doped A4T-16, and 20% PM6 for D18/20 wt% PM6-doped A4T-16) are presented in **Figure 2a**. These profiles demonstrate the suppression effect of PTQ10 and PM6 on the absorption of A4T-16, consistent with the previous discussion. Notably, the reduction in relative absorption intensity in the long wavelength region

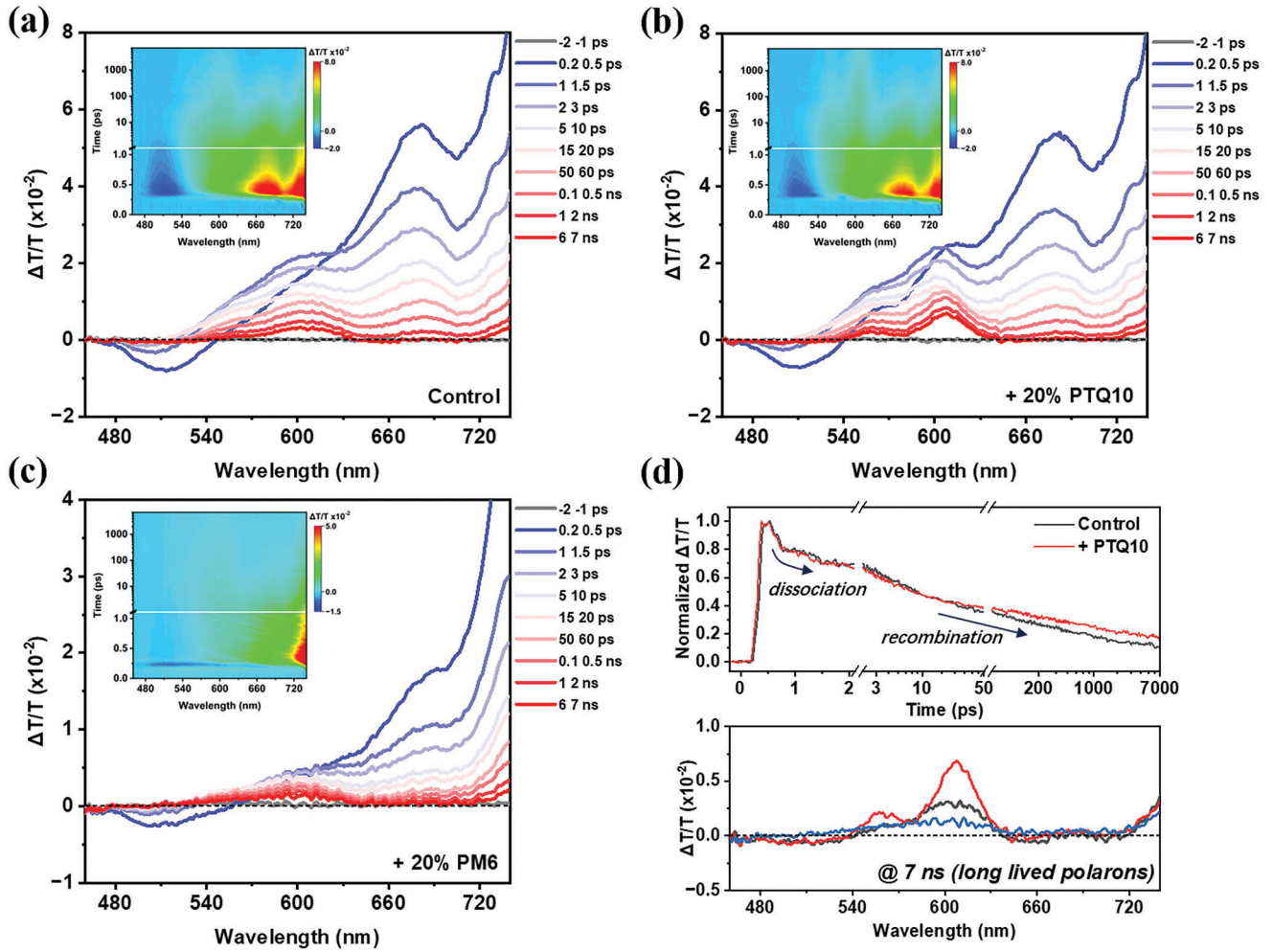

Figure 3. The 2D contour map and representative spectra of fs-TAS for a) control, b) 20% PTQ10, and c) 20% PM6 systems. d) The polaron generation and recombination dynamics and spectra of three systems (blue for the PM6 incorporated one) at 7 ns after excitation.

does not sacrifice charge generation.[58] Next, the current density versus voltage (*J*–*V*) characteristics of devices of ITO/PEDOT:PSS/active layer/PFN-Br/Ag traditional structure are plotted in Figure 2b, with device parameters summarized in **Table 1**. The component optimization details for the PTQ10 introduction are presented in Figure S3 and Table S3 (Supporting Information). Surprisingly, although PTQ10 and PM6 similarly influence the crystallization and aggregation behaviors of A4T-16, their impact on device performance differs significantly. PTQ10 increases the PCE from 15.11% to 16.03%, whereas PM6 reduces the efficiency to 12.78%. This phenomenon deserves more in-depth investigations. To assure the measurement accuracy, the external quantum efficiency (EQE) spectra of the devices are tested and presented in Figure 2c. The integrated current density values in Table 1 confirm that errors are within 5%. EQE spectra indicate that PTQ10 enhances photon conversion, while PM6 decreases the EQE response. Besides, the normal distribution of PCEs for the three systems, based on the results of 15 devices, is presented in Figure 2d, further visualizing the statistical significance of the re-intermixing strategy on the stratified active layer.

Table 1. Device performances.

D18/A4T-16	V_{OC} [V]	J_{SC} [mA cm^{-2}]	*FF* [%]	PCE [%]
Control	0.905	22.08/21.49	75.6	15.11
20% PTQ10	0.912	22.86/22.08	76.9	16.03
20% PM6	0.900	19.42/19.07	73.1	12.78

Before carrying out the deeper morphology characterizations to explain the solar cell efficiency gap, we conducted a series of physical and photo-physical studies on the device. The V_{OC} change exhibited different tendencies for two donor polymers. To analyze energy loss, we used Fourier transform photon spectrum (FTPS) EQE, and EQE-EL.[59,60] As shown in Figure 2e,f, and Table S4 (Supporting Information), the PTQ10-doped device exhibited a significantly lower non-radiative loss, while this reduction is not observed in the PM6 incorporated device, explaining the V_{OC} difference. Next, transient photocurrent (TPC) and photovoltage (TPV) experiments were conducted to evaluate the charge extraction and recombination of the devices, with results

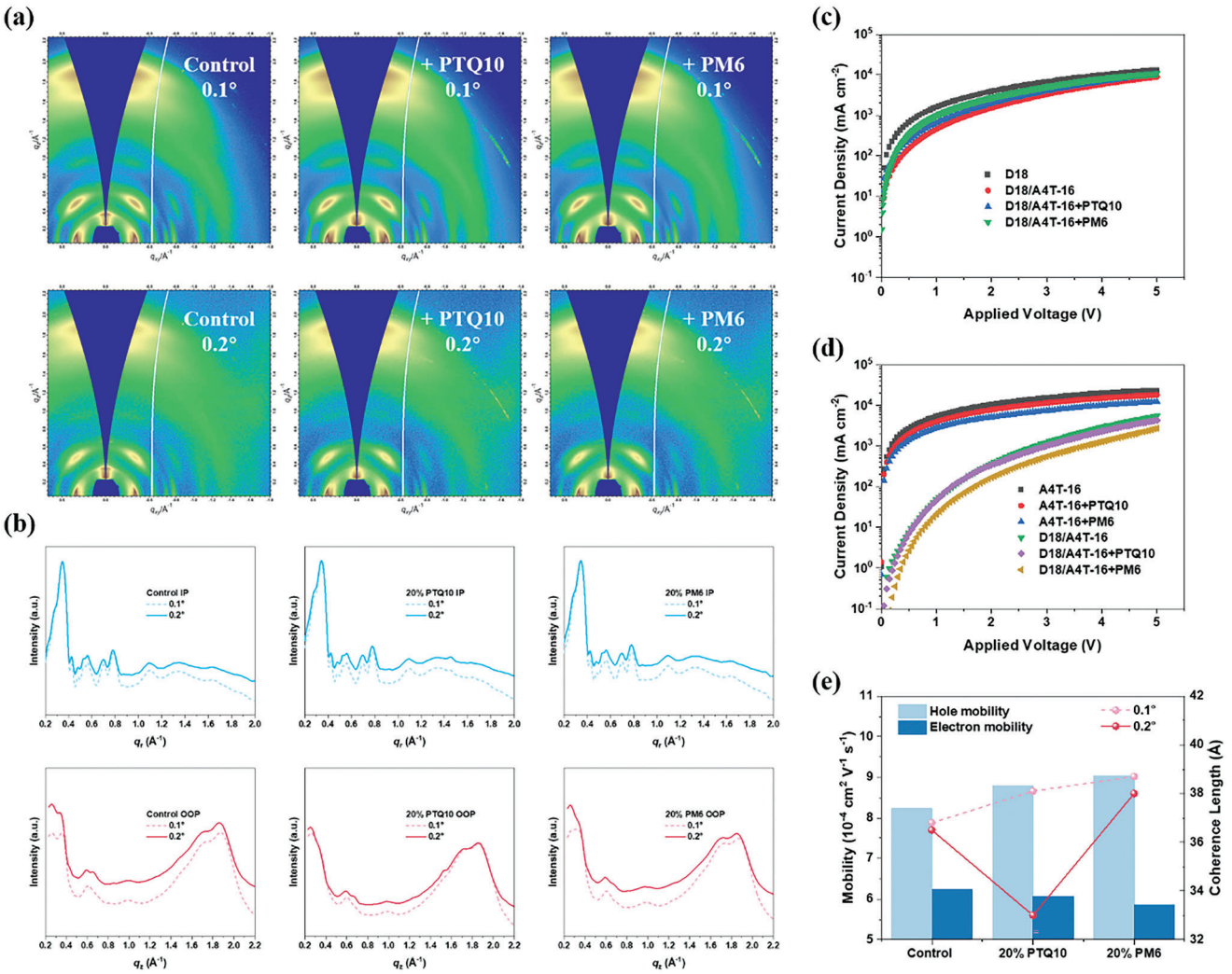

Figure 4. a) 2D GIWAXS patterns of active layers obtained by incidence angles of 0.1° and 0.2°. b) Relative line-cuts of IP and OOP directions. c) Hole-only and d) electron-only device results. e) Mobility and CL values comparison.

shown in Figure 2g–i. According to the calculated results, the charge extraction was less efficient in the devices employing the re-mixing strategy, while the recombination lifetime increased. Apparently, these data cannot directly explain the *FF* change, which will be further discussed after the active layer morphology investigation.

We further investigated the mechanism behind the variation in device FF and Jsc from the perspective of the donor–acceptor interface using the femtosecond transient absorption spectroscopy (fs-TAS) technology.[61–63] TAS spectra of A4T-16 films doped with PTQ10 and PM6 are shown in Figure S4 (Supporting Information), while those of the three active layers are presented in **Figure 3**. Polaron photo-bleaching (PB) features are present in A4T-16+PTQ10 but not in A4T-16+PM6, suggesting that singlet excitons can be dissociated more favorably in A4T-16+PTQ10 samples. This finding is consistent with previous results observed in the A4T-16 neat film.[43] Based on TAS data of the blend films, the 20% PM6 film demonstrates significantly different features in the PB signal region. Thereby, the polaron decay kinetics analysis was only applied to the control film and 20% PTQ10 film, since the 20% PM6 film does not generate a comparable charge population for further comparison. Figure 3d shows the polarons PB kinetics for the control and 20% PTQ10 films. The polarons generation dynamics are comparable, indicating that the improvements in J_{SC} are likely due to the increased donor–acceptor interface area brought by the remixing strategy. Additionally, the recombination dynamics is slower in the 20% PTQ10 film, implying a reduced probability of free charge losses from recombination, thus improving the *FF*. We also analyzed the polaron features obtained from the spectral line cuts at 7 ns. It can be observed that 20% PTQ10 film has a stronger peak intensity at 600 nm (PTQ10-absorption peak in A4T-16 + PTQ10 system) relative to the shoulder at 560 nm (D18 absorption peak). This indicates that positive polarons tend to migrate and potentially interchange between D18 and PTQ10 domains, which may suppress the probability of recombination. Hence, more intense polarons peak intensity remains in 20% PTQ10 film, which also indicates a higher free

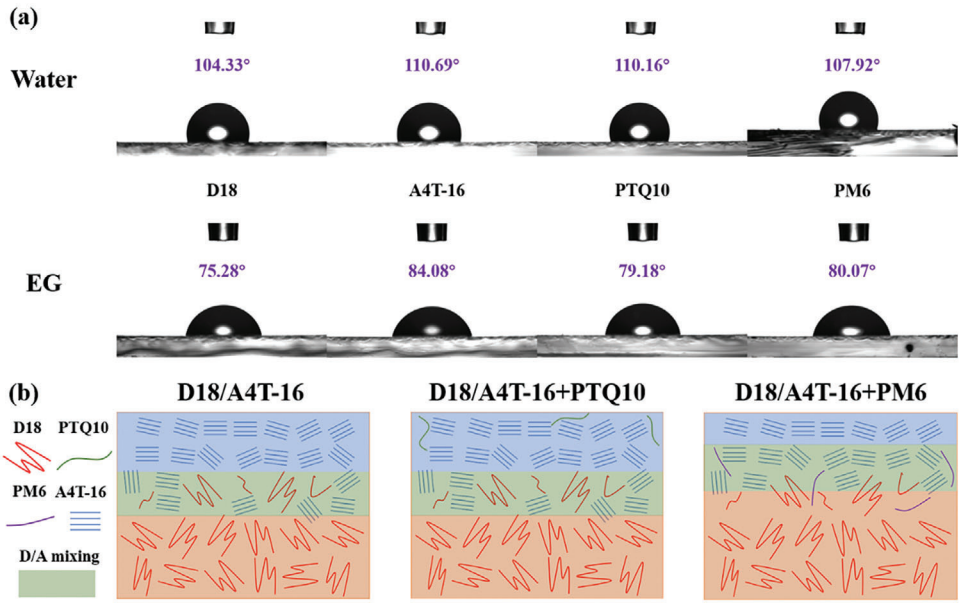

Figure 5. a) Water and ethylene glycol (EG) contact angles upon D18, A4T-16, PTQ10, and PM6 near films. b) Diagram of vertical morphology.

charge population remaining at 7 ns and correlates to reduced recombination.

Then, the active layer morphology was first investigated using the GIWAXS experiment at different incidence angles of 0.1° and 0.2° to assess the crystallization behavior of whole films and their upper part.[64] The derived 2D patterns, line-cuts, and extracted parameters are displayed in **Figure** 4a,b, and Tables S5 and S6 (Supporting Information). The results detected at 0.1° demonstrate overall larger CL values compared to those detected at 0.2° for the A4T-16 signature OOP (010) peaks in all films. This supports the vertical segregation hypothesis: A4T-16 enriches at the top part of the films, resulting in ordered π–π stacking, while the bottom part of the films lacks A4T-16 crystallites, leading to lower CL values. Furthermore, the general crystalline ordering is enhanced by PTQ10 and PM6 doping, especially in the PTQ10-based film, where the CL of IP directional lamellar peak improved to 114.7 Å, compared to the control (109.7 Å) and 20% PM6(111.7 Å). This improvement could be beneficial to achieving more favorable charge transport. To confirm this, the charge mobility of the active layers and related films was assessed by employing the space charge limited current (SCLC) method.[65,66] The hole-only and electron-only device results are plotted in Figure 4c,d, with the calculated hole and electron mobility (μ_h and μ_e) values listed in Table S7 (Supporting Information). Additionally, the μ_h and μ_e values and CL values of the corresponding π–π stacking peak detected at 0.1° and 0.2° are compared in Figure 4e. The introduction of PTQ10 and PM6 enhances the hole mobility of the film due to crystallization regulation and the increase of p-type materials in the films. However, the electron mobility exhibits a decreasing trend with the addition of the two donor polymers. The change in CL values also cannot fully explain the charge mobility variation, indicating that further in-depth investigations through other tests are required.

Next, atomic force microscopy (AFM) and transmission electron microscopy (TEM) measurements are applied to the active layers, as shown in Figure S5 (Supporting Information). AFM height images confirmed that all the films are smooth, and lack nano-fibrillar structures (less efficient charge generation and transport than those based on fused ring acceptors[67]). TEM results suggest that the aggregation motif is influenced by the donor–acceptor remixing strategy: PTQ10 leads to a more sophisticated network while PM6 results in a more separated structure with larger aggregates.

Thanks to varied angle GIWAXS, AFM, and TEM measurements, we noticed that the vertical distribution of A4T-16, D18, and added polymer donors could be reshuffled due to thermodynamical reasons. To investigate this, the surface tensions of the four included materials are evaluated by gauging the water and ethylene glycol (EG) contact angles on the neat films.[68] The stabilized contact angles under all conditions were photographed and are shown in **Figure** 5a, with marked angle values. The surface tensions of the neat films were calculated based on Fowkes and Wu methods, with results demonstrated in Table S8 (Supporting Information). The surface tension values exhibit the following trend:PM6>A4T-16>D18>PTQ10. This implies that after deposition from the solution state,[69] PTQ10 gradually enriches at the top of A4T-16, providing an additional donor-acceptor intermixing region, as visualized in Figure 5b. On the contrary, PM6's larger surface tension indicates that the materials will migrate downward, forming a thicker donor-rich region that harms the electron transfer process without inducing a new donor–acceptor intermixing phase. In this context, the change in charge mobility in the active layer becomes more understandable: top-agglomerated PTQ10 yields poorer donor continuity than PM6 does, thus resulting in lower hole mobility. This morphology-performance relationship demonstrates that studying the entire

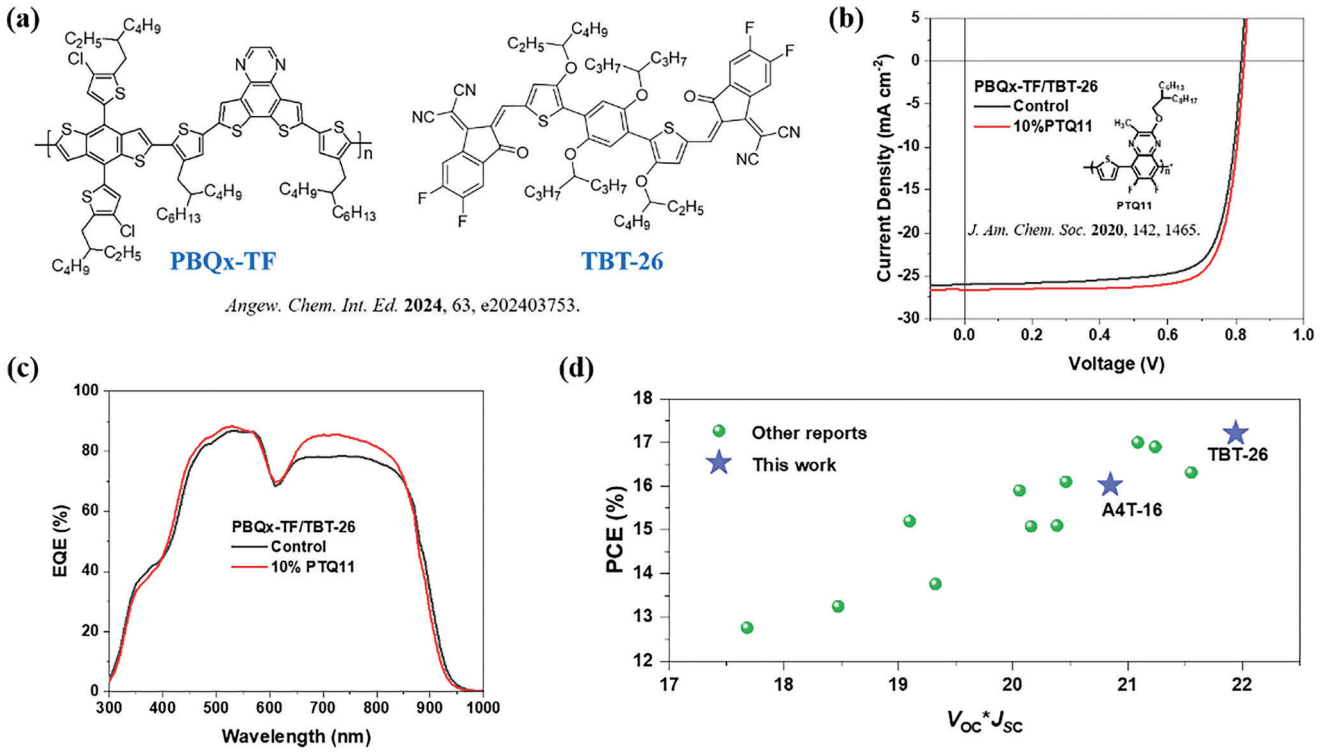

Figure 6. a) Chemical structure of TBT-26. b) *J–V* characteristics, and c) EQE spectra. d) Performance summary of recent advances on completed non-fused acceptor-based OSCs.

film's morphology and optoelectronic properties are insufficient to fully understand donor-acceptor vertically stratified active layers.

Finally, to further explore the effectiveness of our strategy in boosting the performance of low-cost completely non-fused acceptor systems, we selected a recently reported material, TBT-26, along with its pairing donor PBQx-TF (**Figure 6a**).[46] Since our batch of PBQx-TF is not soluble in toluene, or even in hot toluene (due to batch-to-batch difference), the bottom donor layer can be deposited using chlorobenzene (CB) while the top layer can be processed using toluene based on the reported recipe. These procedures would also yield a well-stratified donor–acceptor morphology, allowing PTQ10-series polymers to provide a partially re-intermixing phase in the acceptor-rich region. As a result, PBQx-TF/TBT-26 based devices with 10% additional PTQ11 (better energy level alignment) demonstrated a 17.21% PCE,[70] which is significantly higher than the control of 16.25%, and one of the best efficiencies among completely non-fused ring acceptor-based OSCs.[71–73] These results, including the *J–V* characteristics, EQE spectra, and extracted device parameters, are shown in Figure 6 and **Table 2**, along with the chemical structures of newly mentioned materials. To further emphasize the performance progress, a brief comparison of this work's values with other peers' results on completely non-fused acceptor systems is visualized in Figure 6d, according to detailed information provided in Table S9 (Supporting Information).

Table 2. Device performances.

D18/TBT-26	V_{OC} [V]	J_{SC} [mA cm^{-2}]	*FF* [%]	PCE [%]
Control	0.816	26.00/25.11	76.6	16.25
10% PTQ11	0.824	26.63/25.88	78.4	17.21

3. Conclusion

In summary, to further improve the PCE of the previously established active layer based on a completely non-fused ring acceptor, additional polymer donors are introduced into the acceptor-rich top layer to induce intermixing and stratified morphology. The introduction of PTQ10 successfully formed a remixing phase that served as an additional charge-generation contributor. This system achieved a significantly higher J_{SC}, a slightly enlarged V_{OC}, and an improved *FF* due to suppressed bimolecular recombination, thus enhancing the efficiency from 15.11% to 16.03% for D18(CF)/A4T-16(o-XY) based systems. On the contrary, introducing an equal weight ratio of PM6 led to a decrease in efficiency due to unfavorable vertical active layer morphology. Thereby, this work highlights the importance of a re-intermixing strategy for ideal vertical distribution. Furthermore, by applying this approach to the newly reported PBQx-TF/TBT-26 system, a 17.21% efficiency was realized with the inclusion of 20% PTQ11, representing a cutting-edge level of efficiency for OSCs based on completely non-fused ring acceptors. Such achievements are beneficial to further push the pursuit of carbon neutralization.[74–77]

Supporting Information

Supporting Information is available from the Wiley Online Library or from the author.

Acknowledgements

G.L. thanks for the support from Research Grants Council of Hong Kong (Project Nos 15221320, 15307922, C5037-18G, C4005-22Y), the RGC Senior Research Fellowship Scheme (SRFS2223-5S01), the Hong Kong Polytechnic University: Sir Sze-yuen Chung Endowed Professorship Fund (8-8480), RISE (Q-CDBK), PRI (Q-CD7X), G-SAC5 and the Guangdong-Hong Kong-Macao Joint Laboratory for Photonic-Thermal-Electrical Energy Materials and Devices (GDSTC No. 2019B121205001). R.M. thanks the PolyU Distinguished Postdoctoral Fellowship (1-YW4C). A.K.K. Kyaw thanks the support from the Shenzhen Science and Technology Innovation Commission (JCYJ20220530113014033), the National Natural Science Foundation of China (Grant No. 62150610496,), and the Natural Science Foundation of Guangdong Province. The authors also thank the beamline 7.3.3 at the Advanced Light Source, which is supported by the Director, Office of Science, Office of Basic Energy Sciences, of the U.S. Department of Energy under Contract No. DE-AC02-05CH11231. Dr. Eric Schaible and Dr. Chenhui Zhu at beamline 7.3.3 are also appreciated for assistance with data acquisition.

Conflict of Interest

The authors declare no conflict of interest.

Author Contributions

X.X. performed an investigation, conceptualization, and formal analysis and wrote the final draft. R.M. performed conceptualization, project administration, supervision, and methodology, and wrote, reviewed, and edited the final manuscript. S.Z. and T.A.D.P. performed an investigation and formal analysis. Y.L. and Z.H. performed the investigation. T.J., J.W., Q.F., and W.M. acquired resources. A.K.K.K. and G.L. acquired resources, and funds, and performed supervision, wrote, reviewed, and edited the final manuscript.

Data Availability Statement

The data that support the findings of this study are available from the corresponding author upon reasonable request.

Keywords

completely non-fused ring acceptors, donor/acceptor re-intermixing strategy, organic solar cells, power conversion efficiency, vertical morphology

Received: June 27, 2024
Revised: August 14, 2024
Published online: September 9, 2024

[1] Y. Wang, J. Yu, R. Zhang, J. Yuan, S. Hultmark, C. E. Johnson, N. P. Gallop, B. Siegmund, D. Qian, H. Zhang, Y. Zou, M. Kemerink, A. A. Bakulin, C. Müller, K. Vandewal, X. K. Chen, F. Gao, *Nat. Energy* **2023**, *8*, 978.
[2] Y. Sun, L. Wang, C. Guo, J. Xiao, C. Liu, C. Chen, W. Xia, Z. Gan, J. Cheng, J. Zhou, Z. Chen, J. Zhou, D. Liu, T. Wang, W. Li, *J. Am. Chem. Soc.* **2024**, *146*, 12011.
[3] S. Guan, Y. Li, C. Xu, N. Yin, C. Xu, C. Wang, M. Wang, Y. Xu, Q. Chen, D. Wang, L. Zuo, H. Chen, *Adv. Mater.* **2024**, *36*, 2400342.
[4] L. Tu, H. Wang, W. Duan, R. Ma, T. Jia, T. A. P. Dela Peña, Y. Luo, J. Wu, M. Li, X. Xia, S. Wu, K. Chen, Y. Wu, Y. Huang, K. Yang, G. Li, Y. Shi, *Energy Environ. Sci.* **2024**, *17*, 3365.
[5] Z. Zheng, J. Wang, P. Bi, J. Ren, Y. Wang, Y. Yang, X. Liu, S. Zhang, J. Hou, *Joule* **2022**, *6*, 171.
[6] Y. Wang, S. Zhang, J. Wang, J. Ren, J. Qiao, Z. Chen, Y. Yu, X. T. Hao, J. Hou, *ACS Energy Lett.* **2024**, *9*, 2420.
[7] H. Lu, W. Liu, G. Ran, Z. Liang, H. Li, N. Wei, H. Wu, Z. Ma, Y. Liu, W. Zhang, X. Xu, Z. Bo, *Angew. Chem., Int. Ed.* **2023**, *62*, 202314420.
[8] J. Wang, Z. Zheng, P. Bi, Z. Chen, Y. Wang, X. Liu, S. Zhang, X. Hao, M. Zhang, Y. Li, J. Hou, *Natl. Sci. Rev.* **2023**, *10*, nwad085.
[9] R. Ma, X. Jiang, J. Fu, T. Zhu, C. Yan, K. Wu, P. Müller-Buschbaum, G. Li, *Energy Environ. Sci.* **2023**, *16*, 2316.
[10] X. Yu, P. Ding, D. Yang, P. Yan, H. Wang, S. Yang, J. Wu, Z. Wang, H. Sun, Z. Chen, L. Xie, Z. Ge, *Angew. Chem., Int. Ed.* **2024**, *63*, 202401518.
[11] J. Song, C. Zhang, C. Li, J. Qiao, J. Yu, J. Gao, X. Wang, X. Hao, Z. Tang, G. Lu, R. Yang, H. Yan, Y. Sun, *Angew. Chem., Int. Ed.* **2024**, *63*, 202404297.
[12] G. Ding, T. Chen, M. Wang, X. Xia, C. He, X. Zheng, Y. Li, D. Zhou, X. Lu, L. Zuo, Z. Xu, H. Chen, *Nano-Micro Lett.* **2023**, *15*, 92.
[13] S. Chen, S. Zhu, L. Hong, W. Deng, Y. Zhang, Y. Fu, Z. Zhong, M. Dong, C. Liu, X. Lu, K. Zhang, F. Huang, *Angew. Chem., Int. Ed.* **2024**, *63*, 202318756.
[14] Y. Xin, H. Liu, X. Dong, Z. Xiao, R. Wang, Y. Gao, Y. Zou, B. Kan, X. Wan, Y. Liu, Y. Chen, *J. Am. Chem. Soc.* **2024**, *146*, 3363.
[15] R. Ma, X. Jiang, T. A. Dela Peña, W. Gao, J. Wu, M. Li, S. V. Roth, P. Müller-Buschbaum, G. Li, *Adv. Mater.* **2024**, *36*, 2405005.
[16] Y. Liang, D. Zhang, Z. Wu, T. Jia, L. Lüer, H. Tang, L. Hong, J. Zhang, K. Zhang, C. J. Brabec, N. Li, F. Huang, *Nat. Energy* **2022**, *7*, 1180.
[17] R. Ma, Q. Fan, T. A. Dela Peña, B. Wu, H. Liu, Q. Wu, Q. Wei, J. Wu, X. Lu, M. Li, W. Ma, G. Li, *Adv. Mater.* **2023**, *35*, 2212275.
[18] Y. Li, B. Huang, X. Zhang, J. Ding, Y. Zhang, L. Xiao, B. Wang, Q. Cheng, G. Huang, H. Zhang, Y. Yang, X. Qi, Q. Zheng, Y. Zhang, X. Qiu, M. Liang, H. Zhou, *Nat. Commun.* **2023**, *14*, 1241.
[19] Y. Li, X. Huang, K. Ding, H. K. M. Sheriff, L. Ye, H. Liu, C. Z. Li, H. Ade, S. R. Forrest, *Nat. Commun.* **2021**, *12*, 5419.
[20] K. An, W. Zhong, F. Peng, W. Deng, Y. Shang, H. Quan, H. Qiu, C. Wang, F. Liu, H. Wu, N. Li, F. Huang, L. Ying, *Nat. Commun.* **2023**, *14*, 2688.
[21] R. Po, G. Bianchi, C. Carbonera, A. Pellegrino, *Macromolecules* **2015**, *48*, 453.
[22] T. D. Nielsen, C. Cruickshank, S. Foged, J. Thorsen, F. C. Krebs, *Sol. Energy Mater. Sol. Cells* **2010**, *94*, 1553.
[23] D. J. Burke, D. J. Lipomi, *Energy Environ. Sci.* **2013**, *6*, 2053.
[24] X. Zheng, L. Zuo, K. Yan, S. Shan, T. Chen, G. Ding, B. Xu, X. Yang, J. Hou, M. Shi, H. Chen, *Energy Environ. Sci.* **2023**, *16*, 2284.
[25] X. Gu, Y. Wei, G. Lu, Z. Han, D. Zheng, G. Lu, J. Zhang, Z. Wei, Y. Cai, X. Zhang, H. Huang, *Aggregate* **2023**, *4*, e388.
[26] D. Li, H. Zhang, X. Cui, Y. N. Chen, N. Wei, G. Ran, H. Lu, S. Chen, W. Zhang, C. Li, Y. Liu, Y. Liu, Z. Bo, *Adv. Mater.* **2024**, *36*, 2310362.
[27] D. L. Ma, Q. Q. Zhang, C. Z. Li, *Angew. Chem., Int. Ed.* **2023**, *62*, 202214931.
[28] Z. Han, C. e. Zhang, T. He, J. Gao, Y. Hou, X. Gu, J. Lv, N. Yu, J. Qiao, S. Wang, C. Li, J. Zhang, Z. Wei, Q. Peng, Z. Tang, X. Hao, G. Long, Y. Cai, X. Zhang, H. Huang, *Angew. Chem., Int. Ed.* **2024**, *63*, 202318143.
[29] D. Luo, Z. Jiang, W. L. Tan, L. Zhang, L. Li, C. Shan, C. R. McNeill, P. Sonar, B. Xu, A. K. K. Kyaw, *Adv. Energy Mater.* **2023**, *13*, 2203402.
[30] A. Mishra, G. D. Sharma, *Angew. Chem., Int. Ed.* **2023**, *62*, 202219245.

[31] C. Han, H. Gao, Y. Kan, X. Zhang, X. Jiang, C. Shen, L. Ni, Z. Lv, Z. Zhang, L. Wang, J. A. Zapien, Y. Yang, Y. Sun, K. Gao, *Adv. Energy Mater.* **2024**, *14*, 2304063.
[32] Y. Shao, R. Sun, W. Wang, X. Yang, C. Sun, Y. Li, J. Min, *Sci. China Chem.* **2023**, *66*, 1101.
[33] J. Wang, Y. Wang, J. Li, Y. Yu, P. Bi, J. Qiao, Z. Chen, C. Wang, W. Wang, J. Dai, X. Hao, S. Zhang, J. Hou, *Angew. Chem., Int. Ed.* **2023**, *62*, 202314362.
[34] L. Chen, J. Yi, R. Ma, T. A. Dela Peña, Y. Luo, Y. Wang, Y. Wu, Z. Zhang, H. Hu, M. Li, J. Wu, G. Zhang, H. Yan, G. Li, *Sci. Eng.: R: Rep.* **2024**, *159*, 100794.
[35] M. Nam, C. Lee, D. H. Ko, *Chem. Eng. J.* **2022**, *438*, 135576.
[36] R. Ma, H. Li, T. A. Dela Peña, X. Xie, P. W.-K. Fong, Q. Wei, C. Yan, J. Wu, P. Cheng, M. Li, G. Li, *Adv. Mater.* **2024**, *36*, 2304632.
[37] L. Zhan, S. Li, Y. Li, R. Sun, J. Min, Z. Bi, W. Ma, Z. Chen, G. Zhou, H. Zhu, M. Shi, L. Zuo, H. Chen, *Joule* **2022**, *6*, 662.
[38] R. Ma, C. Yan, P. W.-K. Fong, J. Yu, H. Liu, J. Yin, J. Huang, X. Lu, H. Yan, G. Li, *Energy Environ. Sci.* **2022**, *15*, 2479.
[39] X. Xu, W. Jing, H. Meng, Y. Guo, L. Yu, R. Li, Q. Peng, *Adv. Mater.* **2023**, *35*, 2208997.
[40] P. Wang, J. Zhang, D. Luo, J. Xue, L. Zhang, H. Mao, Y. Wang, C. Yu, W. Ma, Y. Chen, *Adv. Funct. Mater.* **2024**, 2402680.
[41] H. Fu, Z. Peng, Q. Fan, F. R. Lin, F. Qi, Y. Ran, Z. Wu, B. Fan, K. Jiang, H. Y. Woo, G. Lu, H. Ade, A. K. Y. Jen, *Adv. Mater.* **2022**, *34*, 2202608.
[42] M. Xie, L. Zhu, J. Zhang, T. Wang, Y. Li, W. Zhang, Z. Fu, G. Zhao, X. Hao, Y. Lin, H. Zhou, Z. Wei, K. Lu, *Adv. Energy Mater.* **2024**, *14*, 2400214.
[43] X. Xie, R. Ma, Y. Luo, T. A. Dela Peña, P. W.-K. Fong, D. Luo, H. T. Chandran, T. Jia, M. Li, J. Wu, A. K. K. Kyaw, G. Li, *Adv. Energy Mater.* **2024**, 2401355.
[44] L. Wang, C. Chen, Y. Fu, C. Guo, D. Li, J. Cheng, W. Sun, Z. Gan, Y. Sun, B. Zhou, C. Liu, D. Liu, W. Li, T. Wang, *Nat. Energy* **2024**, *9*, 208.
[45] T. A. Dela Peña, R. Ma, Y. Luo, Z. Xing, Q. Wei, Y. Hai, Y. Li, S. A. Garcia, K. L. Yeung, T. Jia, K. S. Wong, H. Yan, G. Li, M. Li, J. Wu, *Adv. Energy Mater.* **2024**, *14*, 2303169.
[46] N. Yang, Y. Cui, Y. Xiao, Z. Chen, T. Zhang, Y. Yu, J. Ren, W. Wang, L. Ma, J. Hou, *Angew. Chem., Int. Ed.* **2024**, *136*, 202403753.
[47] Q. Liu, Y. Jiang, K. Jin, J. Qin, J. Xu, W. Li, J. Xiong, J. Liu, Z. Xiao, K. Sun, S. Yang, X. Zhang, L. Ding, *Sci. Bull.* **2020**, *65*, 272.
[48] L. Ma, S. Zhang, J. Zhu, J. Wang, J. Ren, J. Zhang, J. Hou, *Nat. Commun.* **2021**, *12*, 5093.
[49] W. Wu, Y. Luo, T. A. Dela Peña, J. Yao, M. Qammar, M. Li, H. Yan, J. Wu, R. Ma, G. Li, *Adv. Energy Mater.* **2024**, *14*, 2400354.
[50] Y. Wei, Y. Cai, X. Gu, G. Yao, Z. Fu, Y. Zhu, J. Yang, J. Dai, J. Zhang, X. Zhang, X. Hao, G. Lu, Z. Tang, Q. Peng, C. Zhang, H. Huang, *Adv. Mater.* **2024**, *36*, 2304225.
[51] A. Classen, C. L. Chochos, L. Lüer, V. G. Gregoriou, J. Wortmann, A. Osvet, K. Forberich, I. McCulloch, T. Heumüller, C. J. Brabec, *Nat. Energy* **2020**, *5*, 711.
[52] B. Zou, W. Wu, T. A. Dela Peña, R. Ma, Y. Luo, Y. Hai, X. Xie, M. Li, Z. Luo, J. Wu, C. Yang, G. Li, H. Yan, *Nano-Micro Lett.* **2023**, *16*, 30.
[53] T. A. Dela Peña, R. Ma, Z. Xing, Q. Wei, J. I. Khan, R. M. Young, Y. Hai, S. A. Garcia, X. Zou, Z. Jin, F. L. Ng, K. L. Yeung, D. F. Swearer, M. R. Wasielewski, J. Wang, H. Cha, H. Yan, K. S. Wong, G. Li, M. Li, J. Wu, *Energy Environ. Sci.* **2023**, *16*, 3416.
[54] X. Jiang, A. J. Gillett, T. Zheng, X. Song, J. E. Heger, K. Sun, L. V. Spanier, R. Guo, S. Liang, S. Bernstorff, P. Müller-Buschbaum, *Energy Environ. Sci.* **2023**, *16*, 5970.
[55] W. Gao, R. Ma, T. A. Dela Peña, C. Yan, H. Li, M. Li, J. Wu, P. Cheng, C. Zhong, Z. Wei, A. K. Y. Jen, G. Li, *Nat. Commun.* **2024**, *15*, 1946.
[56] H. Zhang, C. Tian, Z. Zhang, M. Xie, J. Zhang, L. Zhu, Z. Wei, *Nat. Commun.* **2023**, *14*, 6312.
[57] Z. Wang, Z. Peng, Z. Xiao, D. Seyitliyev, K. Gundogdu, L. Ding, H. Ade, *Adv. Mater.* **2020**, *32*, 2005386.
[58] Y. Firdaus, V. M. Le Corre, J. I. Khan, Z. Kan, F. Laquai, P. M. Beaujuge, T. D. Anthopoulos, *Adv. Sci.* **2019**, *6*, 1802028.
[59] Y. Shi, Y. Chang, K. Lu, Z. Chen, J. Zhang, Y. Yan, D. Qiu, Y. Liu, M. A. Adil, W. Ma, X. Hao, L. Zhu, Z. Wei, *Nat. Commun.* **2022**, *13*, 3256.
[60] T. A. Dela Peña, J. I. Khan, N. Chaturvedi, R. Ma, Z. Xing, J. Gorenflot, A. Sharma, F. L. Ng, D. Baran, H. Yan, F. Laquai, K. S. Wong, *ACS Energy Lett.* **2021**, *6*, 3408.
[61] Y. Tamai, Y. Murata, S.-i. Natsuda, Y. Sakamoto, *Adv. Energy Mater.* **2024**, *14*, 2301890.
[62] H. Bai, R. Ma, W. Su, T. A. D. Peña, T. Li, L. Tang, J. Yang, B. Hu, Y. Wang, Z. Bi, Y. Su, Q. Wei, Q. Wu, Y. Duan, Y. Li, J. Wu, Z. Ding, X. Liao, Y. Huang, C. Gao, G. Lu, M. Li, W. Zhu, G. Li, Q. Fan, W. Ma, *Nano-Micro Lett.* **2023**, *15*, 241.
[63] Y. Sun, L. Nian, Y. Kan, Y. Ren, Z. Chen, L. Zhu, M. Zhang, H. Yin, H. Xu, J. Li, *Joule* **2022**, *6*, 2835.
[64] B. Fan, W. Zhong, W. Gao, H. Fu, F. R. Lin, R. W. Y. Wong, M. Liu, C. Zhu, C. Wang, H. L. Yip, F. Liu, A. K. Y. Jen, *Adv. Mater.* **2023**, *35*, 2302861.
[65] D. Jiang, J. Sun, R. Ma, V. K. Wong, J. Yuan, K. Gao, F. Chen, S. K. So, X. Hao, G. Li, H. Yin, *Sci. Eng.: R: Rep.* **2024**, *157*, 100772.
[66] Y. Ma, S. Luan, D. Cai, S. Q. Zhang, J. Y. Wang, Q. Tu, Y. Zhu, Q. Zheng, *Aggregate* **2023**, *4*, e322.
[67] L. Zhu, M. Zhang, J. Xu, C. Li, J. Yan, G. Zhou, W. Zhong, T. Hao, J. Song, X. Xue, Z. Zhou, R. Zeng, H. Zhu, C. C. Chen, R. C. I. MacKenzie, Y. Zou, J. Nelson, Y. Zhang, Y. Sun, F. Liu, *Nat. Mater.* **2022**, *21*, 656.
[68] R. Ma, Y. Tao, Y. Chen, T. Liu, Z. Luo, Y. Guo, Y. Xiao, J. Fang, G. Zhang, X. Li, X. Guo, Y. Yi, M. Zhang, X. Lu, Y. Li, H. Yan, *Sci. China Chem.* **2021**, *64*, 581.
[69] C. Lee, H. Y. Jo, M. Nam, J. Hong, G. H. Kim, H. H. Lee, J. Kim, R. Chang, D. H. Ko, *Adv. Funct. Mater.* **2024**, *34*, 2308047.
[70] C. Sun, S. Qin, R. Wang, S. Chen, F. Pan, B. Qiu, Z. Shang, L. Meng, C. Zhang, M. Xiao, C. Yang, Y. Li, *J Am Chem Society* **2020**, *142*, 1465.
[71] Y. Xiao, H. Yao, J. Wang, T. Zhang, Z. Chen, J. Qiao, N. Yang, Y. Yu, J. Ren, Z. Li, X. Hao, J. Hou, *Adv. Energy Mater.* **2024**, *14*, 2400928.
[72] N. Yang, Y. Cui, T. Zhang, C. An, Z. Chen, Y. Xiao, Y. Yu, Y. Wang, X. T. Hao, J. Hou, *J Am. Chem. Soc.* **2024**, *146*, 9205.
[73] L. Ma, S. Zhang, J. Ren, G. Wang, J. Li, Z. Chen, H. Yao, J. Hou, *Angew. Chem., Int. Ed.* **2023**, *62*, 202214088.
[74] I. McCulloch, M. Chabinyc, C. Brabec, C. B. Nielsen, S. E. Watkins, *Nat. Mater.* **2023**, *22*, 1304.
[75] W. Lin, X. Yao, W. Zhao, Y. Pu, S. Wang, *Green Carbon* **2024**, *2*, 197.
[76] D. Xu, P. Wu, H. Tan, *Information & Functional Materials* **2024**, *1*, 2.
[77] L. Chen, R. Ma, J. Yi, T. A. Dela Peña, H. Li, Q. Wei, C. Yan, J. Wu, M. Li, P. Cheng, H. Yan, G. Zhang, G. Li, *Aggregate* **2024**, *5*, e455.